Colloids and Surfaces B: Biointerfaces 79 (2010) 33–40

Contents lists available at ScienceDirect

Colloids and Surfaces B: Biointerfaces

journal homepage: www.elsevier.com/locate/colsurfb

Preparation of an electrochemical biosensor based on lipid membranes in nanoporous alumina

Jean-Baptiste Largueze[a], Karim El Kirat[b], Sandrine Morandat[a,*]

[a] Université de Technologie de Compiègne – CNRS, UMR 6022 Laboratoire de Génie Enzymatique et Cellulaire, BP 20529, 60205 Compiègne Cedex, France
[b] Université de Technologie de Compiègne – CNRS, UMR 6600 Laboratoire de Biomécanique et Bioingénierie, BP 20529, 60205 Compiègne Cedex, France

ARTICLE INFO

Article history:
Received 25 February 2010
Received in revised form 17 March 2010
Accepted 17 March 2010
Available online 2 April 2010

Keywords:
Biomimetic membrane
Tethered lipid bilayer
Nanoporous electrode
Electrochemistry
Atomic force microscopy
Fluorescence recovery after photobleaching

ABSTRACT

Model lipid bilayers are versatile tools to investigate the molecular processes occurring at the membrane level. Among the model membranes, substrate supported bilayers have attracted much interest because they are robust and they can be investigated by powerful surface sensitive techniques such as electrochemical measurements. In a biosensor, lipid films can be used not only as a support for the biological sensing elements but also as sensing elements themselves to detect molecules that are able to alter the structure and the properties of biomembranes. In this work, we have prepared a tethered lipid membrane-based biosensor able to detect the alterations of membrane structure and fluidity. This tethered lipid membrane was prepared in a nanoporous aluminium oxide that provides a high surface area and a protective environment against dewetting. The membrane contained PEG-PE lipids as hydrating, protective and tethering agents and ubiquinone which is a redox lipophilic mediator embedded within the acyl chains of the lipid bilayer. The lipid membrane was prepared inside the pores of the nanoporous support by a PEG-triggered fusion of liposomes. This sensing system was efficient to detect the alterations of lipid membranes that are induced by the addition of a commonly used non-ionic detergent: Triton X-100.

1. Introduction

Biosensors are analytical devices generally taking advantage of the recognition and/or catalytic properties of biological sensing elements integrated with a signal transducer. The analyte sensing element is a biologically active substance such as an enzyme, antibody, DNA or a microorganism [1]. Biosensors are based on biological elements that are naturally able to perform reagentless molecular biorecognition of specific analytes with high selectivity and sensitivity. In such devices, the molecular recognition should modify the properties of the sensor surface to enable the conversion of biochemical interactions into quantitative electronic information with the help of suitable transducers. Depending on the technique associated with the signal transduction, biosensors can be divided into optical, mass, bioluminescence, electrochemical and thermal sensors. Compared to others, electrochemical biosensors present a good sensitivity, they can operate in turbid solutions and are very stable [2]. In addition, electrochemical biosensors are most commonly used in clinical analysis [1]. Among the electrochemical biosensors, one may distinguish the conductometric, the potentiometric and the amperometric sensors. Compared to potentiometric and conductometric biosensors, the amperometric ones present many advantages such as being more rapid, more sensitive, less expensive and readily disposable [2,3].

Cell membranes act not only as physical barriers to confine cell processes, but they also host much of the machinery for cellular communication and transport across the membrane. The cell membranes are composed of a lipid bilayer with embedded or associated membrane proteins that contribute to specific physiological functions. Model lipid bilayers provide excellent simplified systems to investigate the molecular processes occurring at the membrane level. Among the model membranes, hybrid bilayers (HLBs) are composed of a metal supported alkanethiol self-assembled monolayer (SAM) and a monolayer of phospholipids [4]. These model membranes are very simple to prepare however, the diffusion of lipids is strongly altered by the presence of the SAM monolayer. Furthermore, transmembrane proteins with extra-membranous portions cannot be reconstituted as no water layer is present between the support and the membrane. For these reasons, other more biologically relevant model membranes have been proposed. For instance, supported lipid membranes (SLBs) constitute a biomimetic model which consists in a bilayer deposited directly onto a hydrophilic support such as mica or glass [5–7]. The most prevalent methods used to form SLBs are the Langmuir-Blodgett (LB) technique and the fusion of preformed lipid vesicles. However, there is a significant drawback of SLBs: the thickness of

* Corresponding author. Tel.: +33 3 44 23 44 18; fax: +33 3 44 20 39 10.
E-mail address: sandrine.morandat@utc.fr (S. Morandat).

0927-7765/$ – see front matter © 2010 Elsevier B.V. All rights reserved.
doi:10.1016/j.colsurfb.2010.03.011

the water layer between the solid support and the lower leaflet of the membrane can be inadequate sometimes [8]. Indeed, in some cases the free diffusion of lipids is hindered and some contacts can occur between the support and the extra-membranous portions of membrane proteins. To overcome these drawbacks associated with SLBs and especially to obtain bilayers unstuck from the solid support, tethered lipid bilayers (TLBs) were developed during the last decade [9]. For example, TLBs can be formed by depositing the SLBs onto a polymeric cushion [10–12] or on polyelectrolyte multilayers [13], or even by attaching biotinylated vesicles to the surface using the specific avidin–biotin interaction followed by a fusion step [14,15]. TLBs were often prepared by using tethering lipids that are composed of one terminal group that binds to the substrate, another terminal group that anchors into the bilayer, and an intermediate hydrophilic region (e.g., a polyethylene-glycol (PEG) moiety) [16–18]. In electrochemical applications such as biosensors, the hydrophilic region of tethering lipids can offer the adequate spacing to accommodate extra-membranous portions of membrane proteins and it can also constitute an ion reservoir for electrochemical studies of ion channels and peptides [19–25].

According to the literature, lipid films can be used in a biosensor as a support for the biological sensing elements, especially for membrane-associated proteins [26,27]. In particular, lipid membranes can reduce interferences and unwanted reactions with the sensing surface of the biosensor [28]. However, to our knowledge, lipid films themselves were never used as sensing elements in a biosensor to detect molecules that are able to alter the structure and the properties of biomembranes. In fact, the use of model membranes as sensing elements requires some precautions to preserve their structural and functional properties: the most essential risk for their stability is the dewetting. Protective agents such as sugars can be used to prevent dehydration damages and to increase the stability of model membranes [29,30]. Recently, another air-stable system has been developed by using polyethylene oxide oligomers conjugated to phosphatidylethanolamine lipids (PEG-PE) [31]. The insertion of PEG-PE lipids into the bilayer strongly increased the thickness of the headgroup hydration layer.

In this work, we have prepared a lipid membrane-based biosensor able to detect the alterations of membrane structure and fluidity. This lipid membrane was prepared in a nanoporous aluminium oxide, which provides a high surface to volume ratio and a protective environment against membrane dewetting. The lipid membrane was prepared step-by-step inside the pores of the nanoporous support, with the last step being a PEG-triggered fusion of the surface-attached liposomes. The membrane contained PEG-PE lipids as hydrating, protective and tethering agents and ubiquinone which is a redox lipophilic mediator. This sensing system was efficient to detect the alterations of lipid membranes that are induced by the addition of a common non-ionic detergent: Triton X-100 (TX-100).

2. Experimental

2.1. Materials

Egg yolk L-α-phosphatidylcholine type XVI-E (EggPC), 1,2-dioleyl-sn-glycero-3-phosphatidylethanolamine (DOPE), ubiquinone (co-enzyme Q_{10}, UQ) and L-α-dipalmitoyl-phosphatidylethanolamine-N-NBD (7-nitro-2,1,3-benzoxadiazol-4-yl) (NBD-DPPE), 3-aminopropyl-trietoxy-silane (APTES), N-3-dimethyl-aminopropyl-N′-ethylcarbodiimide (EDC), Triton X-100 (TX-100), polyethylene-glycol 8000 (PEG_{8000}) and 1-undecanethiol were purchased from Sigma–Aldrich (St. Quentin-Fallaviers, France). 1,2-Distearoyl-sn-glycero-3-phosphoethanolamine-N-carboxy-polyethylene-glycol 2000 (DSPE-PEG_{2000}COOH) was from Avanti Polar Lipids (Alabaster, AL, USA). Other chemicals used in this work were all analytical grade and the buffers were prepared with Milli-Q water (resistivity of 18.2 MΩ·cm).

2.2. Preparation of liposomes

Liposomes composed of eggPC/DOPE/DSPE-PEG_{2000}COOH 69:30:1 (mol/mol/mol/mol) (PEG-liposomes), of eggPC/DOPE/DSPE-PEG_{2000}COOH/UQ 67:30:1:2 (mol/mol/mol/mol) (PEG/UQ-liposomes) or of eggPC/DOPE/DSPE-PEG_{2000}COOH/NBD-DPPE 66:30:1:3 (mol/mol/mol/mol) (fluorescent PEG-liposomes) were prepared by sonication. To this end, all components were first dissolved in chloroform. The mixtures were then evaporated under nitrogen and dried in a dessicator under vacuum for 2 h. Multilamellar vesicles (MLV) were obtained by resuspending the lipidic dried film at room temperature in a Hepes buffer (10 mM Hepes, 150 mM NaCl, pH 7.4). The final lipid concentrations were 1.64 mM for PEG- and fluorescent PEG-liposomes and 6.67 mM for PEG/UQ-liposomes. To obtain small unilamellar vesicles (SUVs), the suspension was sonicated to clarity (3 cycles of 2 min 30 s) using a 500 W titanium probe sonicator (Fisher Bioblock Scientific, France; 35% of the maximal power; 13 mm probe diameter) while being kept in an ice bath. The liposomal suspension was then filtered on a 0.2 μm Acrodisc® (Pall Life Sciences, USA) to eliminate titanium particles. Dynamic light scattering (DLS), also known as photon correlation spectroscopy, was used to determine the hydrodynamic diameters of each kind of liposomes. The measurements were performed with the Zetasizer Nano ZS (Malvern Instruments Ltd., UK). The mean hydrodynamic diameter was 83 ± 3 nm for all kinds of liposomes (mean value obtained on 10 independent measurements).

2.3. Preparation of functionalized nanoporous alumina electrodes

Nanoporous alumina electrodes were prepared as described previously [15]. The final alumina electrodes presented the structure drawn in Fig. 1A. SEM images allowed to characterize the dimensions of the nanoporous oxides: the average thickness, the mean diameter of the pores and the average pore density were 11.6 ± 0.5 μm, 184 ± 9 nm and 21.8 pores/μm^2, respectively (data not shown). So the SUVs prepared as described above could easily enter the pores. The Cr/Au layer between the alumina oxide and the electrode is necessary to collect the electric signal from the biomembranes inside the nanopores [15]. This Cr/Au-coated oxide film was connected to the steel wire electrode with the appropriate conductive silver glue to produce a nanoporous electrode (3 mm in diameter) (Fig. 1Aa) [15]. From the geometrical parameters and assuming that the pores are cylindrical, the overall surface area of the pores can be estimated to 9.15 cm^2 per electrode. The electrodes were functionalized by chemisorption of undecanethiol on gold and APTES modification of the alumina walls (Fig. 1Ab and c). First, the electrodes were submitted to UV (254 nm) during 15 min and dipped for 12 h in an ethanol solution containing 1 mM undecanethiol. After thorough rinsing with ethanol, the oxides were dried under nitrogen flow, placed under vacuum with a small vial containing 100 μL of APTES during 30 min at room temperature followed by a curing step of 1 h at 100 °C [32]. Three hundred microliters of the 6.7 mM PEG/UQ-liposomes solution and 100 μL of an EDC solution in Hepes buffer at 1.04 M were then deposited on the top of functionalized nanoporous alumina electrodes (Fig. 1Ad). The electrodes were left overnight at room temperature and protected from light to allow the covalent bonding between the carboxyl function of DSPE-PEG_{2000}COOH and the amine function of APTES. Then, samples were rinsed several times with Hepes buffer and the fusion of the vesicles was triggered by immersing the electrode in 2 mL of a 30% (w/v) PEG_{8000} solution for 15 min (Fig. 1Ae). The

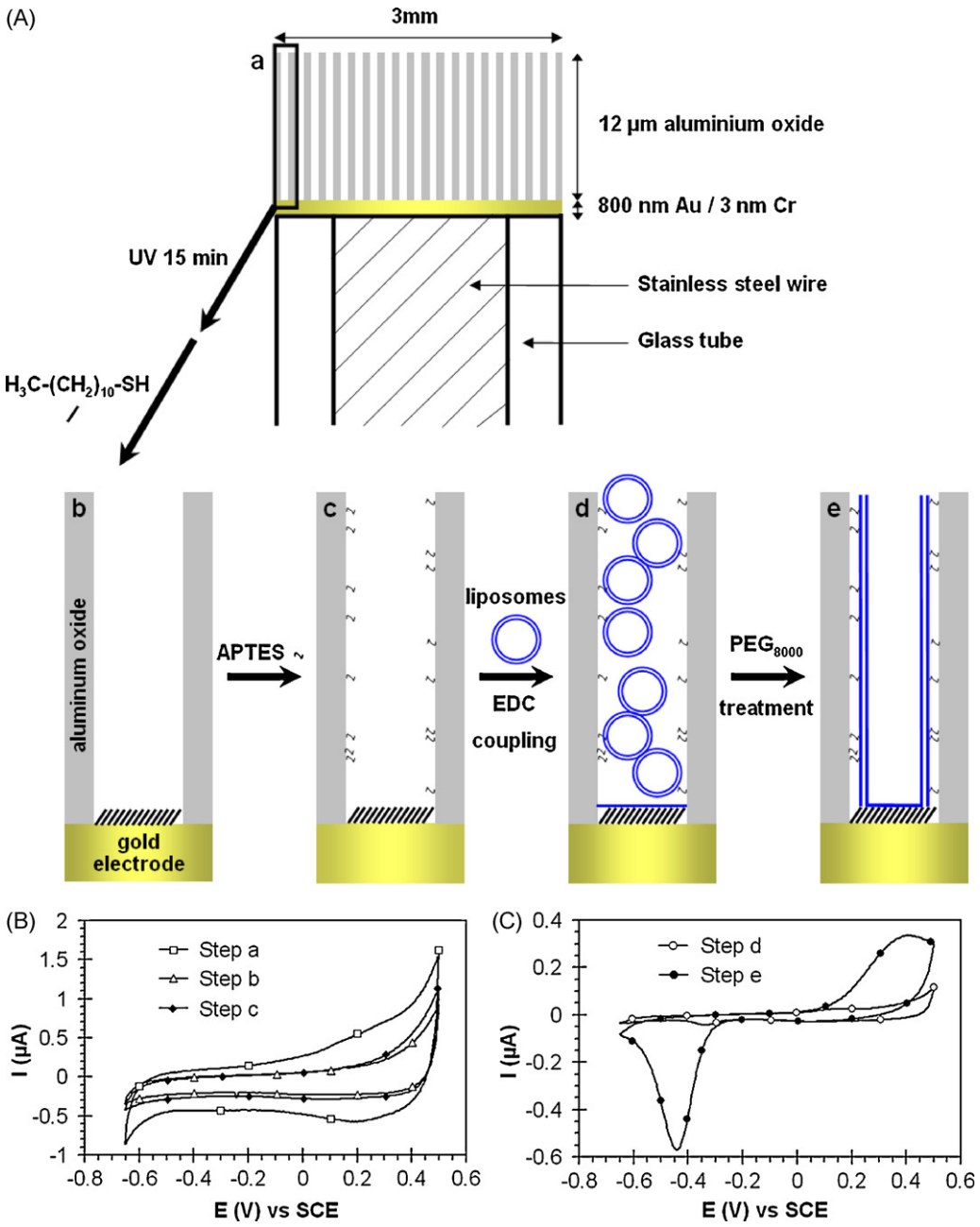

Fig. 1. Preparation of the TLB in the electrode. (A) Step-by-step formation of the PEG-tethered membrane inside the pores of the aluminium oxide. Bare nanoporous electrode structure (step a), the electrode was immersed in an ethanol solution of undecanethiol to functionalize the gold surface (step b) and the alumina surface was modified by vapor deposition of the silane APTES (step c). The electrode was then incubated with EDC and the liposomes presenting free COOH groups, thus resulting in the attachment of the liposomes to the surface of the alumina (step d). The PEG_{8000} treatment permitted to promote the formation of the TLB by membrane fusion (step e). (B) Representative cyclic voltammograms recorded at 50 mV/s in 0.1 mM phosphate buffer pH 7 of the bare electrode, after the self-assembly of the thiol layer on gold and after silanization. (C) Cyclic voltammograms obtained at 5 mV/s for the electrode loaded with liposomes before and after PEG treatment. All the voltammograms were recorded in phosphate buffer 0.1 M pH 7 at 25 °C.

samples were then rinsed extensively with Hepes buffer to remove PEG_{8000} molecules.

2.4. Fluorescence recovery after photobleaching

The lipid bilayers were prepared by the fusion of the fluorescent PEG-liposomes on a glass substrate functionalized with APTES. To do so, 300 µL of fluorescent PEG-liposomes (1.64 mM) and 100 µL of an EDC solution (1.04 M) in Hepes buffer were deposited on the APTES-modified surface and allowed to react overnight at room temperature in obscurity. Then, samples were rinsed several times with Hepes buffer and the fusion of the vesicles was triggered by adding 400 µL of a 30% (w/v) PEG_{8000} solution for 15 min. The PEG_{8000} molecules were removed by rinsing the samples extensively with Hepes buffer.

A commercial confocal scanning light microscope (CSLM) (LSM 410 from Zeiss, Germany) was used for both fluorescence and FRAP measurements. The instrument was composed of an inverted Zeiss microscope (Axiovert 135) equipped with a 40× oil immersion objective (NA 1.3) and with an argon ion laser (488 nm, 15 mW) controlled by the LSM4 software from Zeiss. The glass slide was mounted in an open cell containing 1 mL of Hepes buffer solution covering the supported bilayer. The samples were imaged (310 µm × 310 µm) by collecting the fluorescence emit-

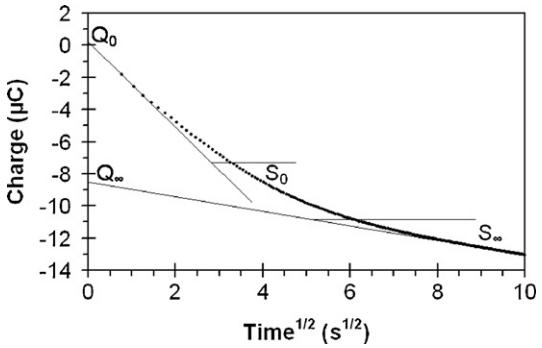

Fig. 2. Typical chronocoulometric plot of UQ diffusion within a lipid bilayer. The UQ pool was first totally oxidized at 0.45 V/SCE. Thereafter, a potential of −0.65 V/SCE was applied while allowing the UQ pool to diffuse inside the membrane during 200 s. The variation of the corresponding reduction charge was followed and plotted versus $(\text{time})^{1/2}$.

ted by the NBD-DPPE probes in bilayers at 525 nm, at a scan speed of 4 s. Control images were first acquired to ascertain the uniformity of fluorescence on each sample. The lateral diffusion coefficient at 25 °C of the fluorescent probe was measured by FRAP after calibration under the conditions detailed previously [33].

2.5. Electrochemical measurements

An anaerobic electrochemical cell was mounted with three electrodes: the working gold-coated porous oxide electrode, a platinum foil auxiliary electrode and a KCl saturated calomel reference electrode (SCE = 0.248 V versus the normal hydrogen electrode at 25 °C). The measuring cell was filled with 50 mL of 0.1 M phosphate buffer pH 7, thermostated at 25 °C by water circulation. For all experiments, the partial pressure of oxygen was reduced by continuously bubbling nitrogen in the buffer. An Autolab PGSTAT12 potentiostat controlled by a PC computer with GPES software (EcoChemie, Utrecht, The Netherlands) was used both for cyclic voltammetry and chronocoulometry. For the chronocoulometry measurements, the quinone pool was first fully oxidized at 0.45 V/SCE during 200 s. Data sampling was performed at the final potential of −0.65 V/SCE with a sampling time of 200 ms. Ubiquinone diffusion coefficients (D_{UQ}) were calculated according to Marchal et al. [34] by using the following formula:

$$D = \frac{1}{4}\pi d^2 \left[\frac{S_0 - S_\infty}{Q_\infty - Q_0}\right]^2$$

where d is the thickness of the alumina oxide, S_0 corresponds to the slope of the reduction current at the initial time, S_∞ is the background slope. Q_0 is the charge corresponding to the adsorption of the redox species at the surface of the electrode, and Q_∞ is the total charge detected. These values were determined as shown on the typical chronocoulometric plot (Fig. 2).

For the experiments of membrane solubilization with TX-100, a first voltammogram was recorded at 5 mV/s before adding the detergent. Then the detergent was injected directly to the desired final concentration into the electrochemical cell with gentle stirring (100 rpm) and a set of ten successive voltammograms (recorded at 5 mV/s) was started 30 s after the injection.

2.6. Atomic force microscopy

The supported lipid bilayers were prepared by the fusion of PEG-liposomes on a mica substrate functionalized with APTES. The attachment of the PEG-liposomes to the APTES-modified mica, and the PEG-triggered fusion were performed as described for the FRAP experiments.

The TLBs were investigated using a commercial AFM (NanoScope III MultiMode AFM, Veeco Metrology LLC, Santa Barbara, CA) equipped with a 125 μm × 125 μm × 5 μm scanner (J-scanner). A quartz fluid cell was used without the O-ring. Topographic images were recorded in contact mode using oxide-sharpened microfabricated Si_3N_4 cantilevers (Microlevers, Veeco Metrology LLC, Santa Barbara, CA) with a spring constant of 0.01 N/m (manufacturer specified), with a minimal applied force (<200 pN) and at a scan rate of 5–6 Hz. The curvature radius of silicon nitride tips was ~20 nm. Images were obtained at room temperature (21–24 °C) in Hepes buffer. All images (256 × 256 pixels) shown in this paper are flattened raw data.

3. Results and discussion

3.1. Electrochemical monitoring of membrane formation inside the nanoporous electrode

Each step of the membrane formation inside the pores was characterized by cyclic voltammetry (Fig. 1). The first step consisted in the functionalization of the gold interface with hydrophobic thiols. The self-assembled thiol layer produced an important decrease of the background signal as compared to the bare electrode (Fig. 1B). The alumina pores were also silanized with APTES. As one can see in the voltammogram, the signal-to-noise ratio was not modified by this treatment which confirms that the gold interface is the sole electrically sensitive part of the electrode [15] (Fig. 1B). In a third step, a mixture of PEG/UQ-liposomes and EDC were added on the electrode. EDC is commonly used to activate terminal carboxyl groups on the DSPE-PEG_{2000}COOH for the conjugation of the liposomes with the amine groups of APTES [35]. At this step, the liposomes were bound to the APTES-modified alumina walls (Fig. 1Ad) as shown by the voltammogram presenting an electrode background current and a small UQ reduction peak at about −0.34 V/SCE (Fig. 1C). A very small charge (0.4 μC) was deduced by integrating this UQ reduction peak. As described previously, UQ is a water insoluble compound, thus it cannot produce any electrochemical reaction in aqueous solutions [14]. Hence, one can deduce that the amount of UQ detected by the electrode only reflects the extent of vesicles fusion on the nanoporous support. Then, the small charge of 0.4 μC corresponds to the spontaneous fusion of some vesicles on the monolayer of thiols covering the gold layer at the pore bottom [15]. Addition of PEG_{8000} to the electrode led to the apparition of an important UQ reduction peak centered at −0.45 V/SCE corresponding to a total charge of 14.25 μC. The UQ charge was determined on at least 10 different electrodes and the mean charge obtained after PEG_{8000} treatment was 11.7 ± 2.6 μC. The charge obtained theoretically (Q_{th}) after liposomes fusion can be estimated from the total area of the pores' walls (by adding the surface of the bottom of the pores (S_b) and the surface of the walls of the pores ($S_w = 0.03 + 9.12 = 9.15\ \text{cm}^2$), the quinone/lipid ratio (2 mol%), and the number of electrons exchanged during the oxidoreduction of UQ ($n_e = 2$) with the formula:

$$Q_{th} = (S_b \times n_{monolayer}/\text{cm}^2 + S_w \times n_{bilayers}/\text{cm}^2) \times \%\,\text{mol}\,UQ \times \Im \times n_e \quad (1)$$

where $n_{monolayer}/\text{cm}^2$ and $n_{bilayer}/\text{cm}^2$ represent the molar quantities of lipids per cm^2 of oxide organized in monolayer and in bilayer respectively. Indeed, if we consider that the fusion of the liposomes led to the formation of a monolayer on hydrophobic alkanethiols [36] and of a bilayer on the hydrophilic alumina substrates [37], we obtained $n_{monolayer}/\text{cm}^2 = 2.44 \times 10^{-10}$ mol/cm^2

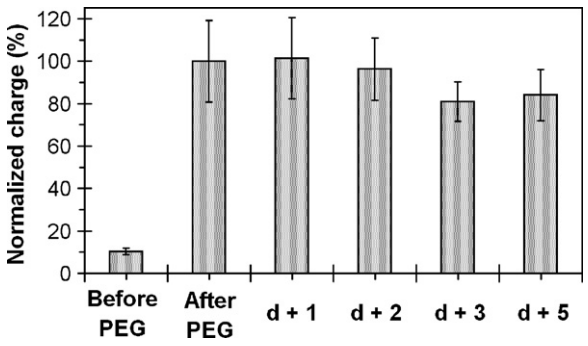

Fig. 3. Stability of the PEG_{2000}-TLBs inside the pores. A set of three electrodes was kept in obscurity and in Tris buffer between each measurement. The cyclic voltammograms were recorded at 5 mV/s every day to determine the remaining charge from the UQ reduction peak. For each electrode, the charge was normalized by taking the initial charge at day zero (i.e., immediately after the PEG treatment) as the reference.

and $n_{bilayer}/cm^2 = 4.88 \times 10^{-10}$ mol/cm^2 (the mean molecular areas were ~73 and 64 Å^2 for eggPC and for DOPE, respectively [38,39]). On the basis of Eq. (1), we have calculated that Q_{th} was approximately 17.2 μC. If we consider the real charge found in the electrode with the standard deviation: 11.7 ± 2.6 μC, we can deduce that the lipid membrane is covering between 53 and 83% of the surface in the electrode. This result could be explained either by an incomplete fusion or by a partial coverage of the membrane (due to a poor accumulation of SUVs in the alumina pores). This charge lower than expected might be due to the geometry of the substrate that is not flat but rather cylindrical or to a misestimation of the total area to cover with the membrane which has been calculated from the geometrical parameters determined on the MEB images. Another reason could be that the fusion is performed with the electrode presenting the pores vertically, so SUVs could sediment and get more concentrated at the bottom of the pores. Finally, there will be less fusion at the top of the electrode.

The stability of the electrode was also verified on several days. TLBs were prepared inside a set of three independent electrodes, the charge due to the reduction of UQ was measured on the first day and during the next 5 days. Before each measurement, the electrodes were dewetted. For each electrode, the charge was normalized by taking the charge obtained immediately after the PEG_{8000}-triggered fusion as the reference. The normalized charges of UQ were plotted versus time (Fig. 3). As one can see, the charge was stable over 5 days after membrane formation and they were resistant to dewetting: the mean charge was always equal or higher than 80% of the initial charge. This result indicates that the TLB-based sensor is stable for days in the nanoporous electrode.

3.2. Validation of the TLBs formation on flat substrates

To prove that the protocol chosen to prepare TLBs in the alumina oxide pores was appropriate, we have performed verifications with FRAP and AFM experiments. Even if it is difficult to consider that membranes on planar surfaces in AFM and FRAP experiments could behave similarly to those in alumina pores, these experiments are useful to verify/visualize membrane formation. A typical fluorescence photobleaching experiment is shown in Fig. 4. Before PEG_{8000} treatment, the absence of fluorescence recovery in the sequence of images suggests that there is no lateral diffusion of the fluorescent lipid probe, thus demonstrating the presence of fluorescent liposomes attached to the surface (Fig. 4A). On the sample treated with PEG_{8000} to trigger membrane fusion, the fluorescence was recovered after few seconds, thereby proving that the fluorescent probe

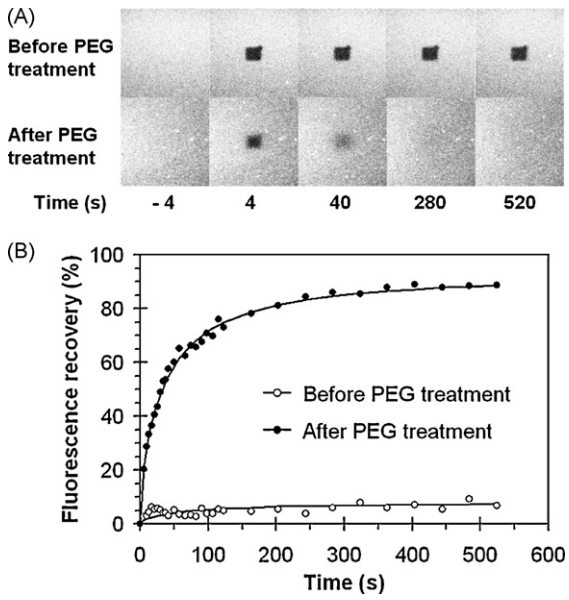

Fig. 4. Characterization of the TLBs by FRAP. (A) FRAP images were recorded before and after the treatment with PEG_{8000}. (B) The experimental data were fitted as described previously [33] to calculate both the diffusion coefficient D ($(3.0 \pm 0.3) \times 10^{-8}$ cm^2/s) and the mobile fraction (93 ± 6%) at 25 °C.

was able to diffuse laterally and that a TLB was formed on the surface (Fig. 4B). After PEG_{8000} addition, the photobleached square was totally refilled with fluorescence within 280 s. The long-range diffusion coefficient and the mobile fraction of the fluorescent lipid were measured from the fluorescence recovery curves as previously described [40] (Fig. 4B). We calculated a mobile fraction and a diffusion coefficient of $\sim 93 \pm 6$% and $(3.0 \pm 0.3) \times 10^{-8}$ cm^2/s, respectively. These values are consistent with the formation of a fluid TLB on the solid support [15,33,41]. However, FRAP experiments are not sufficient to prove the formation of a continuous bilayer, thus AFM imaging was performed with the same preparation protocol of TLBs. Fig. 5 shows the AFM topographic images obtained at different magnifications before and after the PEG_{8000} treatment. Before the addition of PEG_{8000} (Fig. 5A–C), one can observe the presence of aggregated vesicles (dashed circle), holes (full circle) and some bilayer patches (asterisk, thickness of about 5 nm) on the surface. The roughness (RMS value) found for this surface was ~3.8 nm. After the treatment with PEG_{8000} during 15 min, the same sample was thoroughly rinsed and observed again by AFM (Fig. 5D–F). One can observe white dots and a background which is homogeneously grey. Moreover, the roughness of the sample decreased dramatically down to 1.0 nm, thus suggesting the fusion of the liposomes yielded a flatter surface. Another area of the same sample was imaged at higher magnification and some holes were observed (Fig. 5G). Cross sections were measured to determine that the step-height between holes and the grey level was 5.9 ± 0.4 nm, which is consistent with the thickness of a single bilayer [42]. However, the thickness obtained for a supported lipid bilayer composed of fluid PC is 4.4 ± 0.1 nm [42], this indicates that a hydrating compartment of about 1.5 nm is present under the PEG_{2000} tethered bilayer. The white aggregates on the surface are relatively flat and present a thickness of 7.2 ± 0.6 nm which suggests that they may correspond to some patches of a second bilayer.

Altogether, these AFM observations and FRAP experiments allow to conclude that the PEG_{8000}-triggered fusion was efficient and led to the formation of fluid and continuous TLBs. One can then expect that the lipid membrane formed inside the electrodes' pores is organized in a fluid and continuous bilayer.

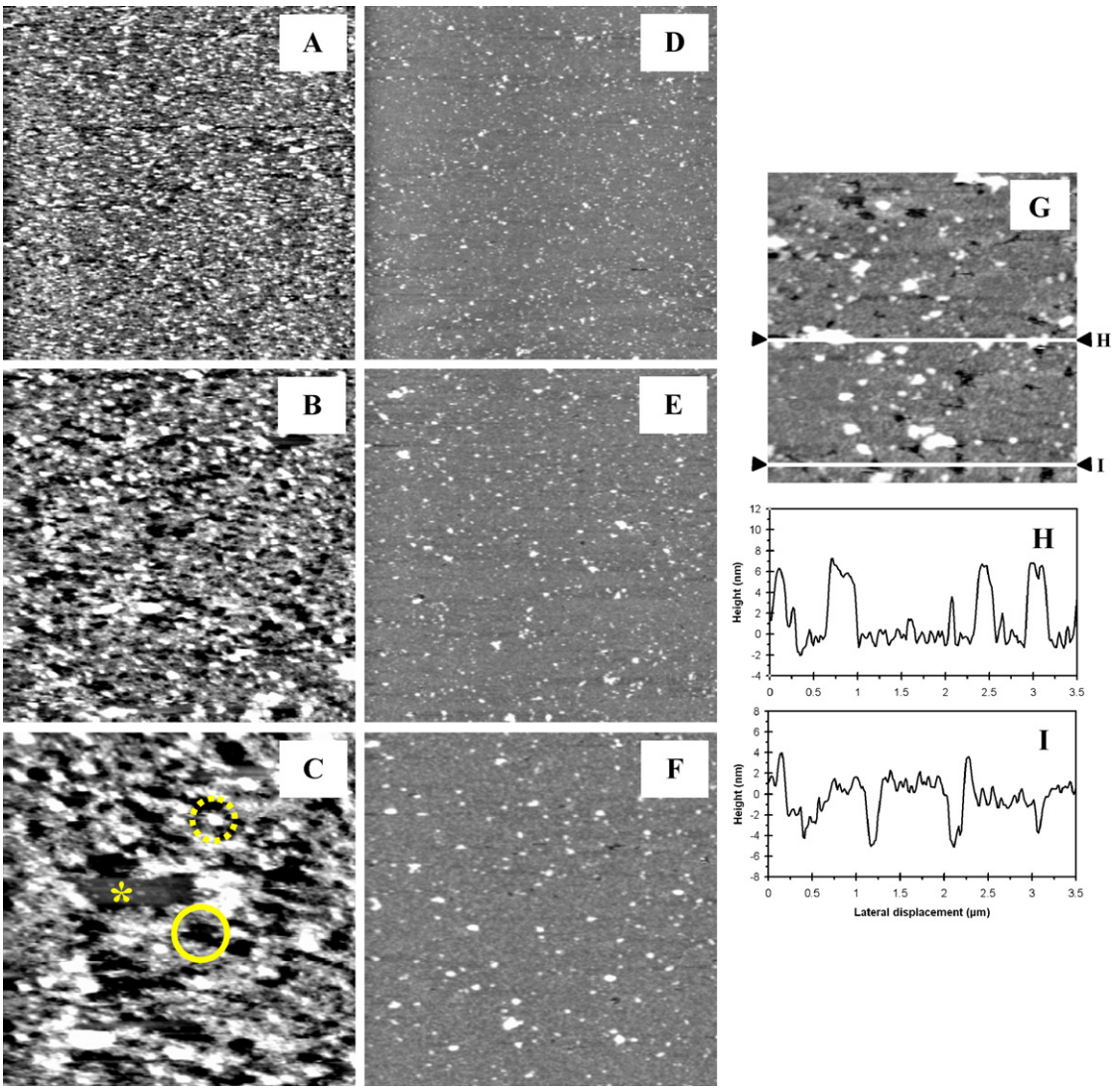

Fig. 5. AFM height images of PEG-liposomes deposited onto mica surfaces silanized with APTES before (A–C) and 15 min after PEG_{8000}-triggered fusion (D–G). The *z*-scale was 10 nm for all images and the sizes were 20 μm × 20 μm (A and D), 10 μm × 10 μm (B and E), 5 μm × 5 μm (C and F) and 3.5 μm × 3.5 μm (G). The following features were added to the image C to indicate some lipid structures: asterisk indicates a bilayer patch, the closed circle shows a hole and the dashed circle is for an aggregate of unfused vesicles. All images were obtained under Hepes buffer at room temperature.

3.3. Electrochemical sensing of membrane solubilization inside the nanoporous electrode

The TLBs were prepared inside the alumina pores and different concentrations of TX-100 were added in the electrochemical cell. Cyclic voltammetry was used to follow the reduction peak of the UQ contained in the bilayers along time after detergent addition. Fig. 6A shows an accumulation of 11 voltammograms recorded before and after the injection of TX-100 at 0.48 mM final concentration (2 times the critical micelle concentration, CMC). The first voltammogram recorded before detergent addition presented an important reduction charge of 14.25 μC. The UQ charge decreased to 11.65 μC immediately after the injection of TX-100 in the electrochemical cell (280 s). The charge obtained from the 3rd voltammogram (740 s after TX-100 injection) was only 6.38 μC traducing an important solubilization of the lipid bilayer. Surprisingly, the charge in the 4th voltammogram (1200 s after TX-100 injection) increased up to 7.55 μC. At 1660s (5th voltammogram), the UQ charge increased again to reach 9.64 μC. This value increased again to reach ~11 μC at 2120s (6th curve), and then it stabilized in all the following measurements. These results suggest that a bilayer formed again on the walls of the pores in the electrode. This is very similar to the progressive redeposition observed previously by AFM during the solubilization of a bilayer with TX-100 [43]. In fact, mixed detergent/lipid/UQ micelles may be able to adsorb progressively on the surface of the alumina walls and lipids may redistribute in a stable bilayer with a little amount of TX-100 remaining. The equilibrium would then be obtained when a part of the lipids/UQ is present on the support in the form of bilayers, and the other part is still in mixed micelles. A control experiment permitted to confirm these conclusions, by introducing PEG/UQ-liposomes pre-solubilized with TX-100 at a concentration of 2CMC, it did not produce a reduction peak. This control suggests that the UQ molecules contained in the mixed micelles were not able to interact with the gold interface in the electrode.

The concentration of TX-100 solutions was varied to solubilize the TLBs in the nanoporous electrode. For all these experiments, the variation of UQ charge induced by the detergent was normalized with the UQ charge of the electrode before TX-100 treatment. The normalized charge was then plotted versus time for each concentration of TX-100 tested (Fig. 6B). As described above for a 2CMC TX-100 concentration, we first observed a decrease of the

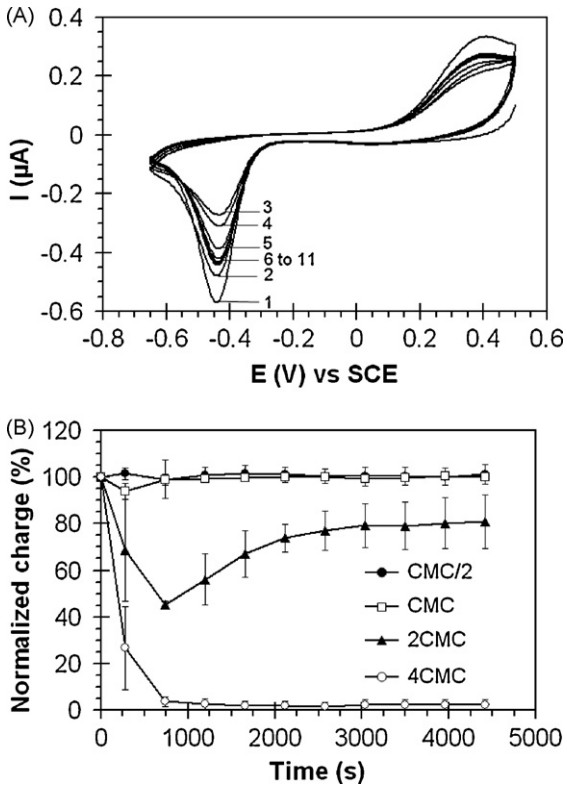

Fig. 6. Electrochemical sensing of membrane solubilization by TX-100. The charge of UQ was followed by cyclic voltammetry at a scan rate of 5 mV/s. Panel A presents the typical voltammograms obtained with TX-100 at 2CMC. A first scan was performed before TX-100 injection (A, curve 1). Then the detergent was injected directly into the electrochemical cell to the desired final concentration and 10 successive scans were recorded to follow the evolution of the UQ reduction peak. (A) For 2CMC, the two earliest scans (A, curves 2 and 3) showed a decrease of UQ reduction signal. During the next scans, the reduction peak increased (A, curves 3–6) to reach a plateau (A, curves 7–11). (B) The normalized total charges obtained from the UQ reduction peak were plotted in function of time to measure membrane perturbation by TX-100. Four different concentrations of TX-100 were tested: CMC/2, CMC (i.e., 0.24 mM), 2CMC and 4CMC.

UQ charge to 45%, then an increase was obtained to finally reach a plateau after ~3000 s at 80%. With 0.96 mM TX-100 (4CMC), the charge of UQ decreased to near zero in 800 s. In this case, the solubilization was completed rapidly, and as seen with the final normalized charge close to zero (0.2 ± 0.1 μC), no redeposition activity was observed. The two other TX-100 concentrations tested CMC (0.24 mM) and CMC/2 (0.12 mM) had no effect on the charge of UQ. This is consistent with the solubilizing properties of detergents observed previously by AFM, for concentrations equal or less than the CMC, they are not able to solubilize lipid membranes [42,43]. We have used potential step chronocoulometry to determine the diffusion coefficients of UQ in the bilayers in the presence of TX-100 at CMC/2 and CMC. Indeed, this is a standard electrochemical technique allowing to determine diffusion coefficients of electroactive species in solution and in lipid membrane assemblies [44]. Similar to the FRAP method, chronocoulometry, provides a measure of the "long-range" diffusion coefficient extending over micrometer distances [34,45]. Table 1 summarizes the different diffusion coefficients calculated for bilayers before and after TX-100 treatment at CMC/2 and CMC. Before the treatment with TX-100, the D_{UQ} was 4.75×10^{-8} cm^2/s, this value is consistent with the literature for the diffusion of UQ in PEG supported bilayers [10] but when streptavidin was used as sublayer, the D_{UQ} measured was lower [15]. This result indicates that the presence of PEG_{2000} molecules under the membrane significantly increased the bilayer fluidity. In the presence of TX-100 at CMC/2 in the electrochemical cell, the

Table 1
Influence of TX-100 on the diffusion coefficient of UQ in the PEG-tethered membranes.

Triton X-100 concentration (mM)	Ubiquinone diffusion coefficient D_{UQ} ($\times 10^{-8}$ cm^2/s)
0	4.75 ± 0.04
0.12 (CMC/2)	4.91 ± 0.04
0.24 (CMC)	5.13 ± 0.08

D_{UQ} increased up to 4.91×10^{-8} cm^2/s, thus suggesting a slight fluidization of the bilayers. The addition of TX-100 at a concentration equal to the CMC provoked an increase of D_{UQ} to 5.13×10^{-8} cm^2/s. These D_{UQ} values indicate that even if TX-100 was not able to solubilize the TLBs at concentrations below the CMC, the fluidity of the membrane was significantly increased by the insertion of detergent molecules. Again these results are consistent with previous AFM observations, calorimetry and infrared spectroscopy studies [42,46].

4. Conclusions

The nanoporous electrode hosting TLBs seems to be a promising easy-to-prepare sensor to study dynamic processes of lipid membrane perturbation. In this work, we have prepared such a biosensor inside the pores of a nanoporous support by a PEG-triggered fusion of liposomes. This sensing system was efficient to detect the alterations of lipid membranes that are induced by the addition of a commonly used non-ionic detergent: Triton X-100. A special feature of this electrode is the possibility to measure the diffusion coefficient in situ, and to quantify the amount of biomembrane that is still unaltered in the electrode in real-time. It will be interesting to discuss the sensitivity of our membrane electrode but there are no comparable sensors in the literature that were used to study membrane alterations/solubilizations.

For instance, one can imagine that this sensing electrode could serve to study the membrane resistance toward detergents, to understand how detergent resistant membranes enriched in sphingomyelin and cholesterol can be formed. Another interesting application would be the study of the enzymatic degradation of lipid bilayer by lipases. The mechanism by which peptides are able to insert in the biomembranes could also be probed with this system. In fact, this electrode would also be useful to detect different membrano-tropic compounds in complex liquid environments.

Acknowledgments

This work was supported by the Université de Technologie de Compiègne, the French Ministry of Research (PPF BIOMIM) and the French Region Picardie (NANOPHARM project). The authors thank Mathieu Haddad and Emilie Froger for their technical assistance and the Service of Physicochemical Analyses of the UTC for providing AFM facilities.

References

[1] J.H. Luong, K.B. Male, J.D. Glennon, Biotechnol. Adv. 26 (2008) 492–500.
[2] M. Mehrvar, M. Abdi, Anal. Sci. 20 (2004) 1113–1126.
[3] E. Bakker, Y. Qin, Anal. Chem. 78 (2006) 3965–3984.
[4] A.L. Plant, Langmuir 15 (1999) 5128–5135.
[5] B. Seantier, M.-C. Giocondi, C. Le Grimellec, P.-E. Milhiet, Curr. Opin. Colloid. Interface Sci. 13 (2008) 326–337.
[6] E.I. Goksu, J.M. Vanegas, C.D. Blanchette, W.C. Lin, M.L. Longo, Biochim. Biophys. Acta 1788 (2009) 254–266.
[7] K. El Kirat, S. Morandat, Y.F. Dufrene, Biochim. Biophys. Acta 1798 (2010) 750–765.
[8] E. Sackmann, Science 271 (1996) 43–48.
[9] C. Rossi, J. Chopineau, Eur. Biophys. J. 36 (2007) 955–965.
[10] B. Deme, D. Marchal, Eur. Biophys. J. 34 (2005) 170–179.
[11] J.C. Munro, C.W. Frank, Langmuir 20 (2004) 10567–10575.

[12] C.A. Naumann, O. Prucker, T. Lehmann, J. Ruhe, W. Knoll, C.W. Frank, Biomacromolecules 3 (2002) 27–35.
[13] R. Kugler, W. Knoll, Bioelectrochemistry 56 (2002) 175–178.
[14] V. Proux-Delrouyre, C. Elie, J.-M. Laval, J. Moiroux, C. Bourdillon, Langmuir 18 (2002) 3263–3272.
[15] O. Fliniaux, C. Elie-Caille, J. Pantigny, C. Bourdillon, Electrochem. Comm. 7 (2005) 697–702.
[16] V. Atanasov, P.P. Atanasova, I.K. Vockenroth, N. Knorr, I. Koper, Bioconjug. Chem. 17 (2006) 631–637.
[17] V. Atanasov, N. Knorr, R.S. Duran, S. Ingebrandt, A. Offenhausser, W. Knoll, I. Koper, Biophys. J. 89 (2005) 1780–1788.
[18] S.M. Schiller, R. Naumann, K. Lovejoy, H. Kunz, W. Knoll, Angew. Chem. Int. Ed. Engl. 42 (2003) 208–211.
[19] S.R. Jadhav, D. Sui, R.M. Garavito, R.M. Worden, J. Colloid Interface Sci. 322 (2008) 465–472.
[20] S.R. Jadhav, Y. Zheng, R.M. Garavito, R.M. Worden, Biosens. Bioelectron. 24 (2008) 837–841.
[21] A. Deniaud, C. Rossi, A. Berquand, J. Homand, S. Campagna, W. Knoll, C. Brenner, J. Chopineau, Langmuir 23 (2007) 3898–3905.
[22] I.K. Vockenroth, P.P. Atanasova, J.R. Long, A.T. Jenkins, W. Knoll, I. Koper, Biochim. Biophys. Acta 1768 (2007) 1114–1120.
[23] L. Becucci, M.R. Moncelli, R. Guidelli, Langmuir 22 (2006) 1341–1346.
[24] L.J. Jeuken, S.D. Connell, P.J. Henderson, R.B. Gennis, S.D. Evans, R.J. Bushby, J. Am. Chem. Soc. 128 (2006) 1711–1716.
[25] P. Yin, C.J. Burns, P.D. Osman, B.A. Cornell, Biosens. Bioelectron. 18 (2003) 389–397.
[26] B.A. Cornell, V.L. Braach-Maksvytis, L.G. King, P.D. Osman, B. Raguse, L. Wieczorek, R.J. Pace, Nature 387 (1997) 580–583.
[27] E. Reimhult, K. Kumar, Trends Biotechnol. 26 (2008) 82–89.
[28] H.T. Tien, A.L. Ottova, Electrochim. Acta 43 (1998) 3587–3610.
[29] S. Chiantia, N. Kahya, P. Schwille, Langmuir 21 (2005) 6317–6323.
[30] S.V. Bennun, R. Faller, M.L. Longo, Langmuir 24 (2008) 10371–10381.
[31] F. Albertorio, A.J. Diaz, T. Yang, V.A. Chapa, S. Kataoka, E.T. Castellana, P.S. Cremer, Langmuir 21 (2005) 7476–7482.
[32] K. El Kirat, M. Bartkowski, K. Haupt, Biosens. Bioelectron. 24 (2009) 2618–2624.
[33] C. Rossi, J. Homand, C. Bauche, H. Hamdi, D. Ladant, J. Chopineau, Biochemistry 42 (2003) 15273–15283.
[34] D. Marchal, W. Boireau, J.M. Laval, J. Moiroux, C. Bourdillon, Biophys. J. 74 (1998) 1937–1948.
[35] S. Zhang, Z. Bian, C. Gu, Y. Zhang, S. He, N. Gu, J. Zhang, Colloid. Surf. B 55 (2007) 143–148.
[36] V.I. Silin, H. Wieder, J.T. Woodward, G. Valincius, A. Offenhausser, A.L. Plant, J. Am. Chem. Soc. 124 (2002) 14676–14683.
[37] R.F. Roskamp, I.K. Vockenroth, N. Eisenmenger, J. Braunagel, I. Koper, Chemphyschem 9 (2008) 1920–1924.
[38] A.B. Serfis, S. Brancato, S.J. Fliesler, Biochim. Biophys. Acta 1511 (2001) 341–348.
[39] J. Schneider, Y.F. Dufrene, W.R. Barger Jr., G.U. Lee, Biophys. J. 79 (2000) 1107–1118.
[40] D. Axelrod, D.E. Koppel, J. Schlessinger, E. Elson, W.W. Webb, Biophys. J. 16 (1976) 1055–1069.
[41] M.E. Johnson, D.A. Berk, D. Blankschtein, D.E. Golan, R.K. Jain, R.S. Langer, Biophys. J. 71 (1996) 2656–2668.
[42] S. Morandat, K. El Kirat, Langmuir 22 (2006) 5786–5791.
[43] K. El Kirat, S. Morandat, Biochim. Biophys. Acta 1768 (2007) 2300–2309.
[44] E. Torchut, J.M. Laval, C. Bourdillon, M. Majda, Biophys. J. 66 (1994) 753–762.
[45] W.L. Vaz, P.F. Almeida, Biophys. J. 60 (1991) 1553–1554.
[46] F.M. Goni, M.A. Urbaneja, J.L. Arrondo, A. Alonso, A.A. Durrani, D. Chapman, Eur. J. Biochem. 160 (1986) 659–665.